Segmenting brain tumors in multi-modal MRI scans using a 3D SegNet architecture

Nabil Jabareen[1 [0000−0002−7847−0075]] and Soeren Lukassen[1 [0000−0001−7045−6327]]

Berlin Institute of Health at Charité - Universitätsmedizin Berlin, Charitéplatz 1, 10117 Berlin, Germany soeren.lukassen@charite.de

Abstract. Gliomas are the most common type of primary brain tumors, and high-grade gliomas are typically treated using a combination of chemotherapy, radiation therapy, and surgical excision. For the latter two therapy options, precise knowledge about the location of the tumor and its components is required, which can be obtained using MRI scans. Manually labeling the tumor area in those 3-dimensional images is a tedious and time-consuming task, hence major efforts have been made to provide automated segmentation. We present our solution to the BraTS 2021 challenge Task1, where we segment gliomas in MRI scans using a SegNet-based approach, achieving competitive and stable performance across tumor types and components. Compared to previous solutions using UNet architectures, our model achieves improved segmentation of the peritumoral edema and comparable performance for the other classes while reducing the number of parameters.

Keywords: Brain Tumors · Deep Learning · Segmentation

1 Introduction

1.1 Gliomas

Gliomas are tumors arising from supporting cells of the brain and represent the most common form of primary brain tumors. Several distinct entities can be distinguished based on their cells of origin and their malignity, with the majority arising from astrocytes (astrocytomas). Among these, glioblastomas (GBMs), also known as grade IV astrocytomas, are both the most common and associated with the worst clinical outcome. Without treatment, the median survival of patients is just 3 months, which can be extended to 15 months through combined treatment with chemotherapeutic agents, radiation, and surgery[8].

Due to the extensive capacity of GBMs to invade the surrounding healthy tissue, as well as the need to destroy as many cancer cells as possible while leaving healthy brain tissue intact, it is vital to obtain a precise localization of the tumor and its sub-regions[16]. At the core of the tumor, there is typically a necrotic zone, caused by nutrient and oxygen starvation in fast-growing tumors (here abbreviated by TC)[14]. This zone is surrounded by living and proliferating tumors cells, the enhancing tumor (ET). As GBMs compromise the integrity

of the blood-brain barrier, the tumor is surrounded by an edema, caused by extravasation of fluid from leaky blood vessels in the tumor's vicinity (WT)[17]. These different tumor compartments can be distinguished by medical imaging. The gold standard for this is multi-modal magnetic resonance imaging (MRI), a technique which delivers images highlighting different structures within soft tissues.

1.2 Segmentation

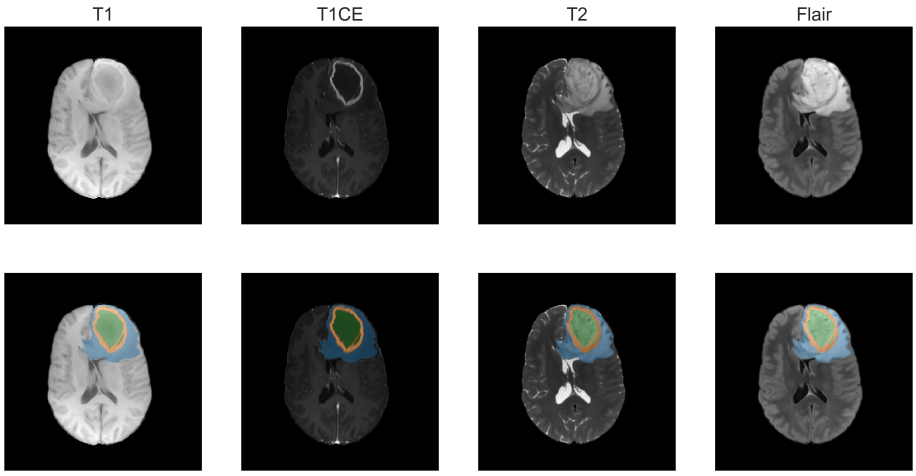

Fig. 1. Four different modalities of MRI scans used for the segmentation. Top row: modalities alone. Bottom row: Superimposed ground truth for segmentation with the peritumoral edema shown in blue, enhancing tumor in red, and necrotic tumor core in green.

Segmentation refers to the task of identifying regions in an image that belong to a certain class, e.g. tumor, healthy tissue, and background. In contrast to object detection, no attempt is made at separating bordering areas belonging to the same class but different entities thereof. Thus, the typical output of a segmentation is a so-called segmentation map, a tensor of the same size as the original image in terms of spatial dimensions, but with one or several channels indicating the presence of certain mutually exclusive or potentially overlapping features, respectively[18]. Due to this relationship of the input and output images, UNet architectures have been exceedingly successful[11]. These convolutional neural networks correspond to an autoencoder-like structure with skip connections between the corresponding encoder and decoder blocks, concatenating the encoder weights to the decoder ones while restoring the image size through transposed

convolutions. The skip connections thus enable the preservation of spatial information[15]. Because max-pooling on the encoder is reversed using transposed convolutions with a receptive field of more than pixel or voxel, some information about maxima is lost during the process. Furthermore, transposed convolutions need to be learned, adding parameters to the model. SegNet architectures aim to alleviate this problem by using unpooling layers instead of transposed convolutions. In these models, the indices of the maxima identified during the max pooling are retained and passed to the unpooling layers, perfectly preserving the localization of the maxima and improving the resolution of the segmentation map[3].

2 Methods

2.1 Data sources

Data used in this publication were obtained as part of the RSNA-ASNR-MICCAI Brain Tumor Segmentation (BraTS) Challenge project through Synapse ID (syn25829067) [4, 12, 5]. 3D Nifti images of size $155 \times 240 times 240$ (Depth x Height x Width) with one channel for each of the four modalities were used as input to the model, while training labels were provided as single-channel Nifti with integer class labels. Example images are shown in figure 1.

2.2 Preprocessing

The data obtained were already skull-stripped, scaled, and cropped as described previously. Our implementation of a SegNet was based on the nnUNet framework, so the additional preprocessing corresponded to that described in [11]. Importantly this includes the cropping of the original input size of $155 \times 255 \times 255$ to $128 \times 128 \times 128$ (see figure 2).

2.3 Network architecture

Table 1. Parameter counts for nnUNet and nnSegNet model architectures.

	nnUNet	nnSegNet
Number of parameters	31,198,176	27,663,648

The proposed nnSegNet architecture is designed to be an efficient deep convolutional neural network for pixel-wise semantic segmentation. It is based on the nnUNet framework [11].
The encoder topology of the nnSegNet consists of five max pooling operations

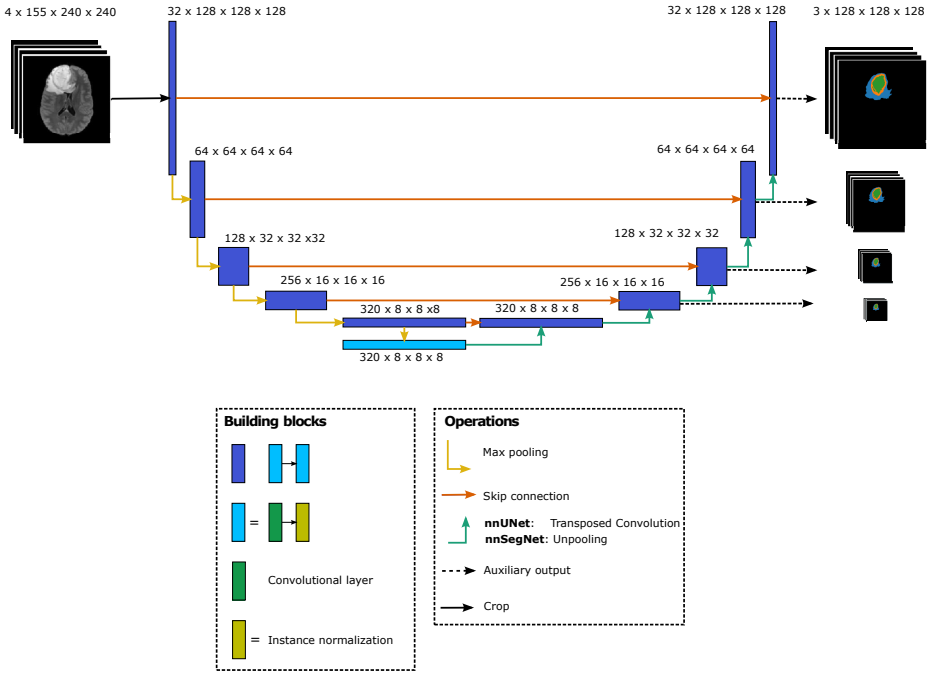

Fig. 2. Depiction of the UNet and SegNet architectures used. Both network types are largely equivalent, with the exception of transposed convolutions in the decoder of the UNet being replaced by unpooling layers in the SegNet (green arrows).

with kernel size of $2\times2\times2$ and a stride of $2\times2\times2$. The indeces of the max pooling operation are saved and later used in the Unpooling operation. The Unpooling operation with a kernel size of $2 \times 2 \times 2$ and stride of $2 \times 2 \times 2$ allows to recreate the feature map size of the corresponding encoder step. The feature map of the corresponding encoder step and the unpooled feature map are concatenated in the decoder part of the network. For a visual comparison of both architectures, see Fig. 2.

2.4 Training

Every network architecture was trained for 1,000 epochs with 250 iterations for each epoch. The initial learning rate was set to 0.01 and a polynomial learning decay was used. As an optimizer we used Stochastic gradient descent with a momentum of 0.99 and weight decay of 3×10^{-5}. To train the model we used deep supervision on auxiliary outputs on different depths of the network (see figure 2).
As a loss function we used a sum of the dice coefficient and the binary cross entropy loss on all auxiliary outputs. The final loss was computed as the weighted sum of all auxiliary losses.

2.5 Postprocessing

To obtain the final prediction we used the computed softmax for every class in a sequential pattern. First, the output mask for the WT class was generated with a given threshold. Second, the output mask for the NC class was generated with a given threshold and the previous mask was overwritten. Finally, this step was repeated for the ET class.
During training the thresholds for all classes were set to 0.5. To improve the final model performance, we optimized the softmax thresholds for every class (see figure 4) on a 5-fold cross validation. For every fold we sampled 1000 different threshold combinations. Due to the interdependence of the different classes and the resulting large search space, we decided to use a Tree-structured Parzen Estimator Approach (TPE) to optimize the thresholds[7]. Finally, we used the median thresholds for every class from all five folds. This optimization has been done separately for the nnSegNet, nnUNet and their Ensemble. We used optuna [2] as optimization framework.
Our second postprocessing step, is aimed to reduce false positive ET predictions. Therefore, we used two thresholds on the predicted ET volume and the predicted NC volume. These thresholds were computed with a decision tree algorithm with a depth of two. Finally, the ET label was suppressed in the final prediction an replaced by the next highest softmax value, if the predicted ET volume was ≤ 129.5 and the NC volume was > 16954.0.

2.6 Metrics

Several metrics were used in the evaluation, specifically the Dice coefficient[9], sensitivity, specificity, and Hausdorff95 distance[13]. The first three are calculated from overlap of sets, with TP indicating true positive, FP false positive, TN true negative, and FN false negative:

$$Dice = \frac{2TP}{2TP + FP + FN} \tag{1}$$

$$Sensitivity = \frac{TP}{TP + FN} \tag{2}$$

$$Specificity = \frac{TN}{TN + FP} \tag{3}$$

The Hausdorff95 distance is defined by the supremum sup of the distance d between two sets X and Y, made more robust to outliers by reporting the $95th$ percentile rather than the maximum:

$$d_{H95} = P_{95}\left\{\sup_{x \in X} d(x, Y), \sup_{y \in Y} d(X, y)\right\} \tag{4}$$

3 Results

3.1 Model architecture

To gauge the performance of existing model architectures, we first trained a UNet using the nnUNet architecture, a frontrunner in previous segmentation challenges. On the training dataset with 5fold cross-validation, this network already outperformed top solution of the past years, likely due to the increased size of the training dataset(Fig. 3)[6, 1].

As with relatively few exceptions the predicted segmentation masks were very close to the ground truth labels, we hypothesized that performance gains could be achieved via smaller adjustments to the network and postprocessing rather than through rewriting the entire architecture. Specifically, we aimed to increase the resolution of the predicted masks while reducing the risk of overfitting. To this end, we replaced the transposed convolutions in the decoder part of the network with unpooling layers, leading to a SegNet architecture(here called nnSegNet due to its integration into the nnUNet framework) which should result in a better conservation of location while also reducing the number of parameters in the model by roughly 10% (Tab. 1)[3]. This resulted in a slight stabilization of the metrics characterized by a lower standard deviation and inter-quartile range of the individual sample scores (Fig. 3).

On the public validation dataset, the performance of the nnSegNet was slightly decreased for the tumor core and enhancing tumor classes, but increased for the peritumoral edema (Tab. 2), with mean scores slightly favoring the nnUNet architecture. An ensemble method combining the predictions of the nnUNet for TC and ET and the nnSegNet for WT did not appear to achieve an overall increase in performance on the training set with cross-validation (Fig. 3).

3.2 Postprocessing

To further improve the performance, we decided to fine-tune the class assignment. As class labels were non-overlapping, it would be possible to use the argmax along the output channels. However, as the classes are nested and predicted with different sensitivities, we took a different approach, sequentially predicting each class to be present if the softmax surpassed a certain threshold (see Methods)[11]. To improve the performance of our model, we decided to tune the threshold for each class, revealing that the previously used threshold of 0.5 is not ideal for all classes (Fig. 4). For ensembles of nnSegNet and nnUNet, this approach was used with the softmax activations for TC and ET from the nnUNet and WT from the nnSegNet, but this did not lead to a major improvement (Figs. 3 and 4).

3.3 Missing classes

For the ET class, we observed a drastic difference of the mean HD95 between the training and validation sets. Upon closer inspection, we found this to be

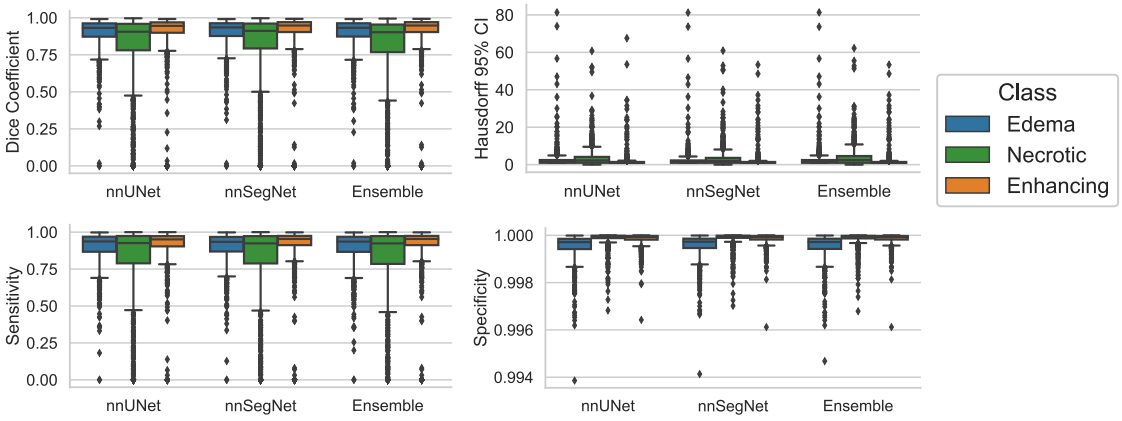

Fig. 3. Performance metrics for different model architectures. Per-image metrics are shown for images from the training dataset, using 5fold cross-validation. Ensemble denotes a combination of nnSegNet activations for the peritumoral edema and nnUNet activations for the other classes. horizontal lines indicate the median, boxes depict the inter-quartile range (IQR), whiskers extend to 1.5x the IQR.

caused by several outliers where ET area was predicted, but was absent from the ground truth annotation. In the metrics calculation for the BraTS challenge, these cases were scored with a HD95 of over 370, resulting in a strong skewing of scores considering the mean score for correctly predicted images was below 10. To address the erroneous prediction of ET voxels in images where no enhancing tumor was present, we made use of the observation that these images typically had very few voxels predicted to be ET, allowing us to set a threshold below which we could reassign the voxels to one of the other two tumor classes or background.

Table 2. Performance metrics for all classes for various model architectures. pp indicates models subjected to threshold tuning and removal of small ET predictions.

Model	Dice WT	Dice ET	Dice TC	HD95 WT	HD95 ET	HD95 TC
nnUNet	0.926	0.816	0.885	3.793	22.873	7.425
nnSegNet	**0.928**	0.808	0.877	3.483	26.232	7.571
Ensemble	0.926	0.808	0.885	3.792	26.231	7.406
nnUNet pp	0.926	**0.848**	0.886	3.783	**9.286**	5.813
nnSegNet pp	**0.928**	0.847	0.878	**3.470**	9.335	7.564
Ensemble pp	0.926	0.843	**0.887**	3.783	9.432	**5.789**

Still, overall scores were strongly influence by poorly performing outliers, as can be seen from the discrepancy of mean and median score values of the nnSegNet (Tab. 3). Similar effects were observed for the other model architectures.

Table 3. Mean vs. median performance metrics for the nnSegNet.

	Dice WT	Dice ET	Dice TC	HD95 WT	HD95 ET	HD95 TC
mean	0.928	0.847	0.878	3.470	9.335	7.564
median	0.948	0.903	0.944	2.236	1.414	1.732

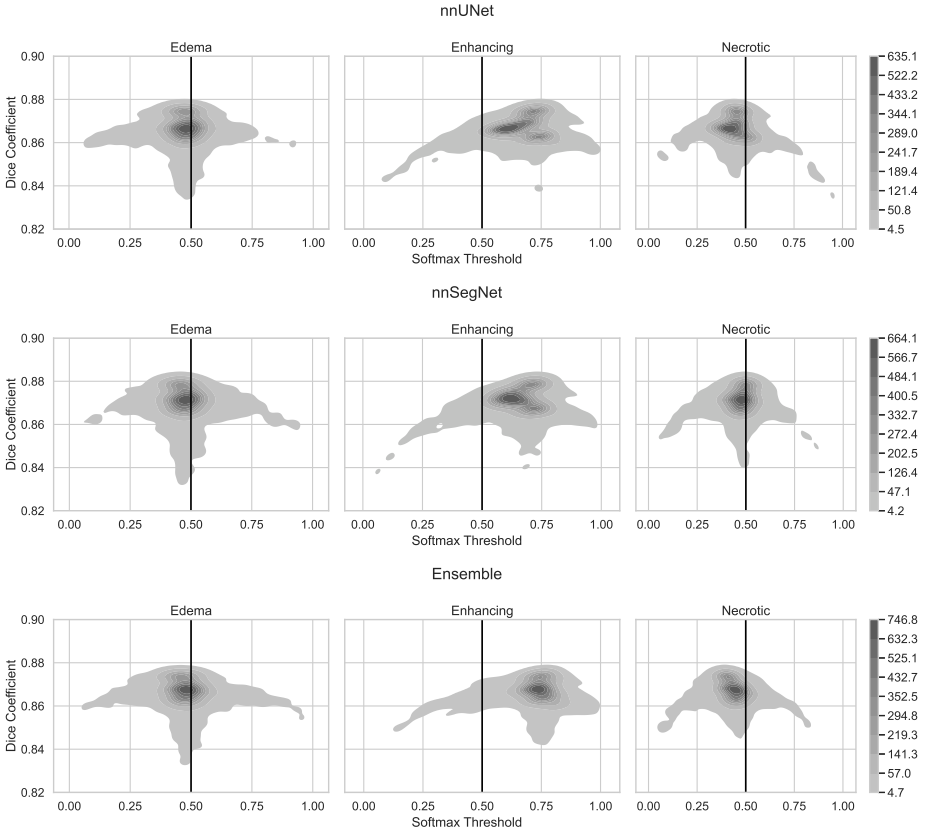

Fig. 4. Threshold optimization. Results of the parameter tuning of thresholds for assigning classes from the softmax activations of the model output. Thresholds are shown on the horizontal axis, Dice coefficients on the vertical axis. Grey levels indicate the density of trials where a corresponding score was achieved. Top row: UNet architecture. Middle row: SegNet architecture. Bottom row: Ensemble with WT from SegNet and the other classes predicted from the UNet activations.

4 Discussion

While the models presented achieve a markedly increased performance compared to previous top competitors, this is in large part due to the increase in samples (660 in 2020, 2,000 in 2021). The nnUNet without post-processing, which is identical to an architecture used for BraTS 2020[10], already performed exceedingly well, with minor performance gains through the post-processing for the WT and TC classes. The nnSegNet architecture did not improve overall results, but achieved a comparable performance with only 88% of the parameters of the nnUNet.

Scores below a Dice coefficient of 0.9 or a Hausdorff95 distance of above 5 were mostly attributable to outliers, indicating that the general performance of the models is exceedingly good. This is also reflected in the median scores of the nnSegNet, ans is especially apparent in the HD95 there. The median HD95 are in the range of 2, which likely falls within the range of disagreement between human specialists. Penalizing the incorrect presence of even a single voxel of e.g. ET in an image where it is absent with a distance of over 370 gives these outlier cases an outsized influence. Since this is the largest possibility for improvement of the segmentation metrics, addressing these outliers above all else is the most promising way to improve the performance in future challenges. To improve the usability in a real-world setting, however, a closer look at common misclassification of e.g. anatomical structures is needed. This is currently disincentivized in challenges, but could be achieved by penalizing the classification of areas such as the choroid plexus as part of the tumor.

5 Acknowledgements

The authors thank Georgios Nikolis for his support with regard to the HPC infrastructure and Foo Wei Ten for fruitful discussions. This work was supported by the German Ministry for Education and Research (BMBF junior research group "Medical Omics", 01ZZ2001).

References

1. Brats2020 validation phase leaderboard. https://www.cbica.upenn.edu/BraTS20/lboardValidation.html, accessed: 2021-08-21
2. Akiba, T., Sano, S., Yanase, T., Ohta, T., Koyama, M.: Optuna: A next-generation hyperparameter optimization framework. In: Proceedings of the 25rd ACM SIGKDD International Conference on Knowledge Discovery and Data Mining (2019)
3. Badrinarayanan, V., Kendall, A., Cipolla, R.: Segnet: A deep convolutional encoder-decoder architecture for image segmentation (2016)
4. Baid, U., Ghodasara, S., Bilello, M., Mohan, S., Calabrese, E., Colak, E., Farahani, K., Kalpathy-Cramer, J., Kitamura, F.C., Pati, S., Prevedello, L.M., Rudie, J.D., Sako, C., Shinohara, R.T., Bergquist, T., Chai, R., Eddy, J., Elliott, J., Reade, W., Schaffter, T., Yu, T., Zheng, J., Annotators, B., Davatzikos, C., Mongan, J., Hess, C., Cha, S., Villanueva-Meyer, J., Freymann, J.B., Kirby, J.S., Wiestler, B., Crivellaro, P., Colen, R.R., Kotrotsou, A., Marcus, D., Milchenko, M., Nazeri, A., Fathallah-Shaykh, H., Wiest, R., Jakab, A., Weber, M.A., Mahajan, A., Menze, B., Flanders, A.E., Bakas, S.: The rsna-asnr-miccai brats 2021 benchmark on brain tumor segmentation and radiogenomic classification (2021)
5. Bakas, S., Akbari, H., Sotiras, A., Bilello, M., Rozycki, M., Kirby, J.S., Freymann, J.B., Farahani, K., Davatzikos, C.: Advancing the cancer genome atlas glioma mri collections with expert segmentation labels and radiomic features. Scientific Data **4**(1), 170117 (Sep 2017). https://doi.org/10.1038/sdata.2017.117, https://doi.org/10.1038/sdata.2017.117
6. Bakas, S., Reyes, M., Jakab, A., Bauer, S., Rempfler, M., Crimi, A., Shinohara, R.T., Berger, C., Ha, S.M., Rozycki, M., Prastawa, M., Alberts, E., Lipkova, J., Freymann, J., Kirby, J., Bilello, M., Fathallah-Shaykh, H., Wiest, R., Kirschke, J., Wiestler, B., Colen, R., Kotrotsou, A., Lamontagne, P., Marcus, D., Milchenko, M., Nazeri, A., Weber, M.A., Mahajan, A., Baid, U., Gerstner, E., Kwon, D., Acharya, G., Agarwal, M., Alam, M., Albiol, A., Albiol, A., Albiol, F.J., Alex, V., Allinson, N., Amorim, P.H.A., Amrutkar, A., Anand, G., Andermatt, S., Arbel, T., Arbelaez, P., Avery, A., Azmat, M., B., P., Bai, W., Banerjee, S., Barth, B., Batchelder, T., Batmanghelich, K., Battistella, E., Beers, A., Belyaev, M., Bendszus, M., Benson, E., Bernal, J., Bharath, H.N., Biros, G., Bisdas, S., Brown, J., Cabezas, M., Cao, S., Cardoso, J.M., Carver, E.N., Casamitjana, A., Castillo, L.S., Catà, M., Cattin, P., Cerigues, A., Chagas, V.S., Chandra, S., Chang, Y.J., Chang, S., Chang, K., Chazalon, J., Chen, S., Chen, W., Chen, J.W., Chen, Z., Cheng, K., Choudhury, A.R., Chylla, R., Clérigues, A., Colleman, S., Colmeiro, R.G.R., Combalia, M., Costa, A., Cui, X., Dai, Z., Dai, L., Daza, L.A., Deutsch, E., Ding, C., Dong, C., Dong, S., Dudzik, W., Eaton-Rosen, Z., Egan, G., Escudero, G., Estienne, T., Everson, R., Fabrizio, J., Fan, Y., Fang, L., Feng, X., Ferrante, E., Fidon, L., Fischer, M., French, A.P., Fridman, N., Fu, H., Fuentes, D., Gao, Y., Gates, E., Gering, D., Gholami, A., Gierke, W., Glocker, B., Gong, M., González-Villá, S., Grosges, T., Guan, Y., Guo, S., Gupta, S., Han, W.S., Han, I.S., Harmuth, K., He, H., Hernández-Sabaté, A., Herrmann, E., Himthani, N., Hsu, W., Hsu, C., Hu, X., Hu, X., Hu, Y., Hu, Y., Hua, R., Huang, T.Y., Huang, W., Huffel, S.V., Huo, Q., HV, V., Iftekharuddin, K.M., Isensee, F., Islam, M., Jackson, A.S., Jambawalikar, S.R., Jesson, A., Jian, W., Jin, P., Jose, V.J.M., Jungo, A., Kainz, B., Kamnitsas, K., Kao, P.Y., Karnawat, A., Kellermeier, T., Kermi, A., Keutzer, K., Khadir, M.T., Khened, M., Kickingereder, P., Kim, G., King, N., Knapp, H., Knecht, U.,

Kohli, L., Kong, D., Kong, X., Koppers, S., Kori, A., Krishnamurthi, G., Krivov, E., Kumar, P., Kushibar, K., Lachinov, D., Lambrou, T., Lee, J., Lee, C., Lee, Y., Lee, M., Lefkovits, S., Lefkovits, L., Levitt, J., Li, T., Li, H., Li, W., Li, H., Li, X., Li, Y., Li, H., Li, Z., Li, X., Li, Z., Li, X., Li, W., Lin, Z.S., Lin, F., Lio, P., Liu, C., Liu, B., Liu, X., Liu, M., Liu, J., Liu, L., Llado, X., Lopez, M.M., Lorenzo, P.R., Lu, Z., Luo, L., Luo, Z., Ma, J., Ma, K., Mackie, T., Madabushi, A., Mahmoudi, I., Maier-Hein, K.H., Maji, P., Mammen, C., Mang, A., Manjunath, B.S., Marcinkiewicz, M., McDonagh, S., McKenna, S., McKinley, R., Mehl, M., Mehta, S., Mehta, R., Meier, R., Meinel, C., Merhof, D., Meyer, C., Miller, R., Mitra, S., Moiyadi, A., Molina-Garcia, D., Monteiro, M.A.B., Mrukwa, G., Myronenko, A., Nalepa, J., Ngo, T., Nie, D., Ning, H., Niu, C., Nuechterlein, N.K., Oermann, E., Oliveira, A., Oliveira, D.D.C., Oliver, A., Osman, A.F.I., Ou, Y.N., Ourselin, S., Paragios, N., Park, M.S., Paschke, B., Pauloski, J.G., Pawar, K., Pawlowski, N., Pei, L., Peng, S., Pereira, S.M., Perez-Beteta, J., Perez-Garcia, V.M., Pezold, S., Pham, B., Phophalia, A., Piella, G., Pillai, G.N., Piraud, M., Pisov, M., Popli, A., Pound, M.P., Pourreza, R., Prasanna, P., Prkovska, V., Pridmore, T.P., Puch, S., Élodie Puybareau, Qian, B., Qiao, X., Rajchl, M., Rane, S., Rebsamen, M., Ren, H., Ren, X., Revanuru, K., Rezaei, M., Rippel, O., Rivera, L.C., Robert, C., Rosen, B., Rueckert, D., Safwan, M., Salem, M., Salvi, J., Sanchez, I., Sánchez, I., Santos, H.M., Sartor, E., Schellingerhout, D., Scheufele, K., Scott, M.R., Scussel, A.A., Sedlar, S., Serrano-Rubio, J.P., Shah, N.J., Shah, N., Shaikh, M., Shankar, B.U., Shboul, Z., Shen, H., Shen, D., Shen, L., Shen, H., Shenoy, V., Shi, F., Shin, H.E., Shu, H., Sima, D., Sinclair, M., Smedby, O., Snyder, J.M., Soltaninejad, M., Song, G., Soni, M., Stawiaski, J., Subramanian, S., Sun, L., Sun, R., Sun, J., Sun, K., Sun, Y., Sun, G., Sun, S., Suter, Y.R., Szilagyi, L., Talbar, S., Tao, D., Tao, D., Teng, Z., Thakur, S., Thakur, M.H., Tharakan, S., Tiwari, P., Tochon, G., Tran, T., Tsai, Y.M., Tseng, K.L., Tuan, T.A., Turlapov, V., Tustison, N., Vakalopoulou, M., Valverde, S., Vanguri, R., Vasiliev, E., Ventura, J., Vera, L., Vercauteren, T., Verrastro, C.A., Vidyaratne, L., Vilaplana, V., Vivekanandan, A., Wang, G., Wang, Q., Wang, C.J., Wang, W., Wang, D., Wang, R., Wang, Y., Wang, C., Wang, G., Wen, N., Wen, X., Weninger, L., Wick, W., Wu, S., Wu, Q., Wu, Y., Xia, Y., Xu, Y., Xu, X., Xu, P., Yang, T.L., Yang, X., Yang, H.Y., Yang, J., Yang, H., Yang, G., Yao, H., Ye, X., Yin, C., Young-Moxon, B., Yu, J., Yue, X., Zhang, S., Zhang, A., Zhang, K., Zhang, X., Zhang, L., Zhang, X., Zhang, Y., Zhang, L., Zhang, J., Zhang, X., Zhang, T., Zhao, S., Zhao, Y., Zhao, X., Zhao, L., Zheng, Y., Zhong, L., Zhou, C., Zhou, X., Zhou, F., Zhu, H., Zhu, J., Zhuge, Y., Zong, W., Kalpathy-Cramer, J., Farahani, K., Davatzikos, C., van Leemput, K., Menze, B.: Identifying the best machine learning algorithms for brain tumor segmentation, progression assessment, and overall survival prediction in the brats challenge (2019)

7. Bergstra, J., Bardenet, R., Bengio, Y., Kégl, B.: Algorithms for hyper-parameter optimization. In: Shawe-Taylor, J., Zemel, R., Bartlett, P., Pereira, F., Weinberger, K.Q. (eds.) Advances in Neural Information Processing Systems. vol. 24. Curran Associates, Inc. (2011), https://proceedings.neurips.cc/paper/2011/file/86e8f7ab32cfd12577bc2619bc635690-Paper.pdf

8. Brodbelt, A., Greenberg, D., Winters, T., Williams, M., Vernon, S., Collins, V.P.: Glioblastoma in england: 2007–2011. European Journal of Cancer **51**(4), 533–542 (2015). https://doi.org/https://doi.org/10.1016/j.ejca.2014.12.014, https://www.sciencedirect.com/science/article/pii/S0959804915000039

9. Dice, L.R.: Measures of the amount of ecologic association between species. Ecology **26**(3), 297–302 (1945). https://doi.org/https://doi.org/10.2307/1932409, https://esajournals.onlinelibrary.wiley.com/doi/abs/10.2307/1932409
10. Isensee, F., Jaeger, P.F., Full, P.M., Vollmuth, P., Maier-Hein, K.H.: nnu-net for brain tumor segmentation (2020)
11. Isensee, F., Jaeger, P.F., Kohl, S.A.A., Petersen, J., Maier-Hein, K.H.: nnu-net: a self-configuring method for deep learning-based biomedical image segmentation. Nature Methods **18**(2), 203–211 (Feb 2021). https://doi.org/10.1038/s41592-020-01008-z, https://doi.org/10.1038/s41592-020-01008-z
12. Menze, B.H., Jakab, A., Bauer, S., Kalpathy-Cramer, J., Farahani, K., Kirby, J., Burren, Y., Porz, N., Slotboom, J., Wiest, R., Lanczi, L., Gerstner, E., Weber, M.A., Arbel, T., Avants, B.B., Ayache, N., Buendia, P., Collins, D.L., Cordier, N., Corso, J.J., Criminisi, A., Das, T., Delingette, H., Demiralp, c., Durst, C.R., Dojat, M., Doyle, S., Festa, J., Forbes, F., Geremia, E., Glocker, B., Golland, P., Guo, X., Hamamci, A., Iftekharuddin, K.M., Jena, R., John, N.M., Konukoglu, E., Lashkari, D., Mariz, J.A., Meier, R., Pereira, S., Precup, D., Price, S.J., Raviv, T.R., Reza, S.M.S., Ryan, M., Sarikaya, D., Schwartz, L., Shin, H.C., Shotton, J., Silva, C.A., Sousa, N., Subbanna, N.K., Szekely, G., Taylor, T.J., Thomas, O.M., Tustison, N.J., Unal, G., Vasseur, F., Wintermark, M., Ye, D.H., Zhao, L., Zhao, B., Zikic, D., Prastawa, M., Reyes, M., Van Leemput, K.: The multimodal brain tumor image segmentation benchmark (brats). IEEE Transactions on Medical Imaging **34**(10), 1993–2024 (2015). https://doi.org/10.1109/TMI.2014.2377694
13. Pompeiu, D.: Sur la continuité des fonctions de variables complexes. In: Annales de la Faculté des sciences de Toulouse: Mathématiques. vol. 7, pp. 265–315 (1905)
14. Rong, Y., Durden, D.L., Van Meir, E.G., Brat, D.J.: 'Pseudopalisading' Necrosis in Glioblastoma: A Familiar Morphologic Feature That Links Vascular Pathology, Hypoxia, and Angiogenesis. Journal of Neuropathology & Experimental Neurology **65**(6), 529–539 (06 2006). https://doi.org/10.1097/00005072-200606000-00001, https://doi.org/10.1097/00005072-200606000-00001
15. Ronneberger, O., Fischer, P., Brox, T.: U-net: Convolutional networks for biomedical image segmentation (2015)
16. Weller, M., van den Bent, M., Preusser, M., Le Rhun, E., Tonn, J.C., Minniti, G., Bendszus, M., Balana, C., Chinot, O., Dirven, L., French, P., Hegi, M.E., Jakola, A.S., Platten, M., Roth, P., Rudà, R., Short, S., Smits, M., Taphoorn, M.J.B., von Deimling, A., Westphal, M., Soffietti, R., Reifenberger, G., Wick, W.: Eano guidelines on the diagnosis and treatment of diffuse gliomas of adulthood. Nature Reviews Clinical Oncology **18**(3), 170–186 (Mar 2021). https://doi.org/10.1038/s41571-020-00447-z, https://doi.org/10.1038/s41571-020-00447-z
17. Wolburg, H., Noell, S., Fallier-Becker, P., Mack, A.F., Wolburg-Buchholz, K.: The disturbed blood–brain barrier in human glioblastoma. Molecular Aspects of Medicine **33**(5), 579–589 (2012). https://doi.org/https://doi.org/10.1016/j.mam.2012.02.003, https://www.sciencedirect.com/science/article/pii/S0098299712000180, water Channel Proteins (Aquaporins and Relatives)
18. Yang, R., Yu, Y.: Artificial convolutional neural network in object detection and semantic segmentation for medical imaging analysis. Frontiers in Oncology **11**, 573 (2021). https://doi.org/10.3389/fonc.2021.638182, https://www.frontiersin.org/article/10.3389/fonc.2021.638182